Intracellular pH-regulating Mechanism of the Squid Axon

Interaction between DNDS and Extracellular Na^+ and HCO_3^-

WALTER F. BORON and ROGER C. KNAKAL

From the Department of Cellular and Molecular Physiology, Yale University School of Medicine, New Haven, Connecticut 06510

ABSTRACT Intracellular pH (pH_i) of the squid axon is regulated by a stilbene-sensitive transporter that couples the influx of Na^+ and HCO_3^- (or the equivalent) to the efflux of Cl^-. According to one model, the extracellular ion pair $NaCO_3^-$ exchanges for intracellular Cl^-. In the present study, the ion-pair model was tested by examining the interaction of the reversible stilbene derivative 4,4'-dinitrostilbene-2,2'-disulfonate (DNDS) with extracellular Na^+ and HCO_3^-. Axons (initial $pH_i \sim 7.4$) were internally dialyzed with a pH 6.5 solution containing 400 mM Cl^- but no Na^+. After pH_i, as measured with a glass microelectrode, had fallen to ~6.6, dialysis was halted. In the presence of both external Na^+ and HCO_3^- ($pH_o = 8.0$, 22°C), pH_i increased due to the pH_i-regulating mechanism. At a fixed $[Na^+]_o$ of 425 mM and $[HCO_3^-]_o$ of 12 mM, DNDS reversibly reduced the equivalent acid-extrusion rate (J_H) calculated from the rate of pH_i recovery. The best-fit value for maximal inhibition was 104%, and for the $[DNDS]_o$ at half-maximal inhibition, 0.3 mM. At a $[Na^+]_o$ of 425 mM, the $[HCO_3^-]_o$ dependence of J_H was examined at 0, 0.1, and 0.25 mM DNDS. Although J_{max} was always ~20 pmol cm^{-2} s^{-1}, $K_m(HCO_3^-)$ was 2.6, 5.7, and 12.7 mM, respectively. Thus, DNDS is competitive with HCO_3^-. At a $[HCO_3^-]_o$ of 12 mM, the $[Na^+]_o$ dependence of J_H was examined at 0 and 0.1 mM DNDS. Although Jmax was ~20 pmol cm^{-2} s^{-1} in both cases, $K_m(Na^+)$ was 71 and 179 mM, respectively. At a $[HCO_3^-]_o$ of 48 mM, J_{max} was ~20 pmol cm^{-2} s^{-1} at $[DNDS]_o$ levels of 0, 0.1, and 0.25 mM. However, $K_m(Na^+)$ was 22, 45, and 90 mM, respectively. Thus, DNDS (an anion) is also competitive with Na^+. The results are consistent with simple competition between DNDS and $NaCO_3^-$, and place severe restrictions on other kinetic models.

INTRODUCTION

The intracellular pH (pH_i) of the squid giant axon, like that of the snail neuron (Thomas, 1977) and giant barnacle muscle fiber (Boron et al., 1981), is regulated by

Address reprint requests to Dr. Walter F. Boron, Department of Cellular and Molecular Physiology, Yale University School of Medicine, 333 Cedar Street, P.O. Box 3333, New Haven, CT 06510-2989.

J. GEN. PHYSIOL. © The Rockefeller University Press · 0022-1295/89/01/0123/28 $2.00

Volume 93 January 1989 123–150

a Na^+-dependent Cl-HCO_3 exchanger. In response to intracellular acid loads, this transporter mediates the uptake of Na^+ and HCO_3^- (or an equivalent species), and the efflux of Cl^- (for reviews, see Roos and Boron, 1981; Thomas, 1984). The stoichiometry is one mole of Na^+ taken up for each mole of Cl^- lost, and for every two equivalents of acid neutralized inside the cell (Boron and Russell, 1983). However, the mechanism by which Na^+ and the acid-base equivalents are transported across the membrane remains to be established. Among the possibilities (see Boron, 1985) are that (*a*) one Na^+ and one HCO_3^- enter, and one H^+ exits; (*b*) one Na^+ and two HCO_3^- enter; (*c*) one Na^+ and one $CO_3^=$ enter; and (*d*) one $NaCO_3^-$ ion pair enters.

The likelihood of the above alternatives was examined in an earlier kinetic study of the acid-extrusion rate (i.e., equivalent H^+ efflux, J_H) in the squid axon (Boron, 1985). It was found that when $[HCO_3^-]_o$ is varied, the apparent maximal J_H (J_{max}) is independent of $[Na^+]_o$, but that the apparent K_m for HCO_3^- ($K_m[HCO_3]$) is inversely proportional to $[Na^+]_o$. Conversely, $J_{max}(Na)$ is independent of $[HCO_3^-]_o$, but $K_m(Na)$ is inversely proportional to $[HCO_3^-]_o$. Furthermore, when the J_H data were plotted as a function of the calculated $[NaCO_3^-]_o$, all the data fell along the same curve, regardless of whether the $[HCO_3^-]_o$ was varied at various fixed values of $[Na^+]_o$, or vice versa. These results were consistent with the $NaCO_3^-$ ion-pair model, and placed restrictions on other kinetic models.

In the present work, we further test the ion-pair model by exploring the effect of 4,4′-dinitrostilbene-2,2′-disulfonate (DNDS) on the axon's pH_i-regulating system. Acid-extrusion rates were calculated from rates of pH_i recovery from acid loads in internally dialyzed squid axons. We found that DNDS, which is a divalent anion, is a reversible inhibitor of acid extrusion. In experiments in which we examined J_H as a function of $[HCO_3^-]_o$ at different values of $[DNDS]_o$, we found that this stilbene appears to be a simple competitive inhibitor with respect to HCO_3^-. Similarly, in experiments in which we examined J_H as a function of $[Na^+]_o$, we found that DNDS appears to be competitive with respect to Na^+. These results are consistent with the $NaCO_3^-$ ion-pair model, and place severe restrictions on other kinetic models.

Portions of this work have been reported in preliminary form (Boron and Knakal, 1985).

METHODS

General

The experiments were conducted at the Marine Biological Laboratory, Woods Hole, MA, during May and June, 1984. Live specimens of the squid *Loligo paelei* were decapitated, and the first stellar nerve from each side was removed and placed in cold (~4°C) Woods Hole seawater. A 4–5-cm length of giant axon (generally 400–600-μm diameter) was isolated from the nerve by microdissection, and cannulated horizontally in a chamber (see Boron and Russell, 1983) designed for internal dialysis (Brinley and Mullins, 1967). A length of dialysis tubing (see below) was threaded through one cannula, down the length of the axon, and out the opposite cannula. In addition, pH- and voltage-sensitive microelectrodes were introduced through opposite cannulas, so that their tips were within 500 μm of one another at the middle of the axon. Artificial seawater continuously flowed around the axon. The temperature, controlled by a circulating water bath connected to the water jacket on the underside of the chamber, was 22°C.

Solutions

The standard extracellular fluid (i.e., artificial seawater, ASW) had the following nominal composition (in millimolar): 425.2 Na^+, 12 K^+, 3 Ca^{++}, 57.5 Mg^{++}, 531 Cl^-, 12 HCO_3^-, 0.1 $EDTA^=$, 15 of the anionic form of [2-hydroxyethyl]-1-piperazine-propane sulfonic acid (EPPS), and 15 of the neutral form of EPPS (pK ~8.0). The pH was 8.00 and the osmolality was ~980 mosmol/kg. ASW was delivered to the chamber through CO_2-impermeable Saran tubing (Clarkson Equipment and Controls, Detroit, MI). When $[Na^+]_o$ was lowered, Na^+ was replaced mole for mole by *N*-methyl-D-glucammonium, made by titrating the free base (Sigma Chemical Co., St. Louis, MO) with HCl. When $[HCO_3^-]_o$ was varied, HCO_3^- was exchanged for Cl^- on a mole-for-mole basis.

The HCO_3^--containing seawaters were made as described previously (Boron, 1985). Throughout this paper, the $[HCO_3^-]_o$ values reported are nominal values. However, because some of the added HCO_3^- went on to form CO_2, $CO_3^=$, and various ion pairs (i.e., $NaCO_3^-$, $MgCO_3$, $CaCO_3$), the actual $[HCO_3^-]_o$ values were probably ~10% less than the nominal values. See Appendix 1 for a derivation of the equations describing the fate of HCO_3^- added to aqueous solutions.

In the initial and final phases of each experiment, the axons were exposed to HCO_3-free ASW. This was similar to the standard ASW except that it contained no HCO_3^- (Cl^- replacing HCO_3^-), only 10 mM K^+, and only 10 mM total EPPS ($MgCl_2$ replacing MgEPPS on an osmole-for-osmole basis).

The internal dialysis fluid (DF) had the following composition (in millimolar): 0 Na^+, 415.3 K^+, 7 Mg^{++}, 8 Tris, 400 Cl^-, 14 glutamate, 4 $ATP^=$, 1 $EGTA^=$, 13.3 of the anionic form of 2-[*N*-morpholino]-ethanesulfonic acid (MES), 6.7 of the neutral form of MES, 215 glycine, and 0.5 phenol red. The pH was adjusted to 6.5 with HCl or KOH, and osmolality was adjusted to ~980 mosmol/kg with glycine. The ATP was added to the DF on the day of the experiment from a 400-mM stock solution (pH 7.0) that was stored at −5°C.

Internal Dialysis

Internal dialysis (Brinley and Mullins, 1967) permits control of the intracellular ionic environment. Details on our use of this technique can be found in earlier papers (Boron and Russell, 1983; Boron, 1985). The dialysis capillaries were made from cellulose acetate tubing (Fisher Research Laboratories, Inc., Dedham, MA) having an outer diameter of 140 μm. An 18-mm length of this tubing was rendered permeable to low molecular weight solutes by hydrolyzing it in 0.1 N NaOH for 18–24 h. The dialysis capillaries were perfused with DF at a rate of ~5 μl/min.

Measurement of pH_i

The pH-sensitive microelectrodes were of the design of Hinke (1967). They were constructed of lead glass (0120; Corning Glass Works, Corning, NY) and pH-sensitive glass (Clark Electromedical Instruments, Pangbourne, England). Details on the construction of these microelectrodes, the electrical arrangements, and the control of the experiments by computer can be found in earlier papers (Boron and Russell, 1983; Boron, 1985).

Calculation of Acid Extrusion Rates

We define the acid extrusion rate (J_H) as the net flux of H^+ out of the cell plus the flux of HCO_3^- (or other alkali equivalents) into the cell. The experimental protocol was to lower pH_i by dialyzing the axon with a low-pH solution, and then halt dialysis. The subsequent pH_i recovery rate (dpH_i/dt) was used to compute J_H, which was taken as the product of dpH_i/dt,

the total intracellular buffering power (as modified by the presence of CO_2/HCO_3^-), and the axon diameter (see Boron, 1985). For each axon, J_H was determined for up to four external solutions, one of which was always our standard ASW, which had the following composition: $[Na^+]_o$ = 425 mM, $[HCO_3^-]_o$ = 12 mM, pH_o = 8.00, and $[DNDS]_o$ = 0. Each of the calculated J_H values was divided by the J_H value obtained under these standard conditions to yield normalized J_H values, as described previously (Boron, 1985). This normalization procedure reduces the scatter of the data, but sometimes necessitates special curve-fitting routines, as described below.

Curve-fitting Procedures

We used various nonlinear least-squares methods to curve fit our J_H data. Data pertaining to the reduction of J_H by extracellular DNDS (i.e., percent inhibition vs. $[DNDS]_o$) was fitted with a standard Michaelis-Menten curve using an iterative procedure (Scarborough, 1966). The other original J_H data reported in this paper can be grouped into eight series: (1) J_H vs. $[HCO_3^-]_o$ at 425 mM Na^+/0 mM $[DNDS]_o$, (2) the same at 0.1 mM DNDS, (3) the same at 0.25 mM DNDS, (4) J_H vs. $[Na^+]_o$ at 12 mM $[HCO_3^-]_o$/0 mM DNDS, (5) the same at 12 HCO_3^-/0.1 DNDS, (6) the same at 48 HCO_3^-/0 DNDS, (7) the same at 48 HCO_3^-/0.1 DNDS, and (8) the same at 48 HCO_3^-/0.25 DNDS. Data from each of these eight series of experiments were individually fitted to a standard Michaelis-Menten equation (see Segel, 1975), or to a modified form in which the curve was forced through an arbitrary point (Boron, 1985). The curve-fitting approach was the iterative approach noted above (Scarborough, 1966).

The eight fitting procedures described above yielded best-fit values for the apparent maximal J_H (J_{max}) and apparent K_m values for either Na^+ or HCO_3^-, but only at a single $[DNDS]_o$. Because apparent J_{max} and K_m ought to be independent of $[DNDS]_o$, one could simultaneously fit data from experiments at two or three values of $[DNDS]_o$ to an equation of the form:

$$J_H = J^S_{max} \frac{[S]_o}{[S]_o + K^S_m (1 + [DNDS]_o/K_i)}, \quad (1)$$

where $[S]_o$ is the concentration of the varied external substrate (i.e., either Na^+ or HCO_3^-), J^S_{max} is the apparent maximal flux when $[S]_o$ is varied, and K^S_m is the apparent Michaelis constant for S. The advantage of this approach is that single best-fit values are obtained for J^S_{max}, K^S_m, and K_i. Because the J_H data for each experiment were normalized to the mean J_H (i.e., 16.8 ± 0.5 pmol cm^{-2} s^{-1}, n = 169) obtained under "standard" conditions (i.e., $[HCO_3^-]_o$ = 12 mM, $[Na^+]_o$ = 425 mM, and $[DNDS]_o$ = 0) in this study, the fitted curve must be forced through this standard point ($[HCO_3^-]_o$ = 12 mM, $[Na^+]_o$ = 425 mM, and $[DNDS]_o$ = 0, J_H = 16.8 pmol cm^{-2} s^{-1}). This was accomplished by fitting the data to the following variant of Eq. 1:

$$J_H = \frac{[S]_o}{[S]_o + K^S_m (1 + [DNDS]_o/K_i)} \cdot \frac{J'_H(S' + K^s_m)}{S'}, \quad (2)$$

where J'_H is the value of J_H that prevails under standard conditions (i.e., 16.8 pmol cm^{-2} s^{-1}), and S' is $[S]_o$ under standard conditions (i.e., 425 mM when S is Na^+, and 12 mM when S is HCO_3^-). In deriving Eq. 2, we assumed that $[DNDS]_o$ = 0 under standard conditions. When data are fitted to Eq. 2, the result is best-fit values for the apparent K^s_m and K_i. J_{max} is calculated from the relation:

$$J_{max} = \frac{J'_H(S' + K^s_m)}{S'} \quad (3)$$

Simultaneous fittings of data were performed for three groups of results: (*a*) experiments in which $[HCO_3^-]_o$ was varied at 425 mM $[Na^+]_o$ at three $[DNDS]_o$ levels (series 1–3); (*b*) experiments in which $[Na^+]_o$ was varied at 12 mM $[HCO_3^-]_o$ at two $[DNDS]_o$ levels (series 4 and 5); and (*c*) experiments in which $[Na^+]_o$ was varied at 48 mM $[HCO_3^-]_o$ at three $[DNDS]_o$ levels (series 6–8).

Finally, data from all eight series of experiments (348 points at various values of $[HCO_3^-]_o$, $[Na^+]_o$, and $[DNDS]_o$ were simultaneously fitted to each of four rapid-equilibrium kinetic models (see Discussion). We found that, with the approach described by Scarborough (1966), the fits did not converge for the more complex of these models. Therefore, we employed an iterative approach in which we systematically varied each of the fitted parameters, minimizing the sum of squares of residuals. Although this least-squares fitting approach is time consuming and does not yield the standard deviations of the fitted parameters, it always converges.

Previously Reported Data

Two series of data used in the present analysis were previously reported (Boron, 1985). These are the data for series 1 (J_H vs. $[HCO_3^-]_o$ at 425 mM Na^+/0 mM $[DNDS]_o$) and the data for series 4 (J_H vs. $[Na^+]_o$ at 12 mM $[HCO_3^-]_o$/0 mM DNDS). Because the data from each axon were normalized to the same standard condition, both in the previous study and in the present one, the fact that the data from series 1 and 4 were obtained in a different year from those of the other series should not affect our analysis. In addition, our analysis of rapid-equilibrium kinetic models (see Discussion) includes four other series of data, all obtained in the absence of DNDS, from the earlier study (Boron, 1985): (A) J_H vs. $[HCO_3^-]_o$ at 212 mM Na^+, (B) J_H vs. $[HCO_3^-]_o$ at 106 mM Na^+, (C) J_H vs. $[Na^+]_o$ at 6 mM HCO_3^-, and (D) J_H vs. $[Na^+]_o$ at 3 mM HCO_3^-.

Statistics

The apparent K_m and J_{max} values, derived from iterative least-squares curve fits (see above), are given ± the standard deviation. Mean values of acid extrusion rates and pH_i are given ± the standard error.

RESULTS

Effect of DNDS on pH_i Recovery from an Acid Load

Fig. 1 illustrates the results of an experiment in which the internal dialysis technique was used to impose an intracellular acid load on a squid axon. Throughout the experiment, pH_o was 8.00 and $[Na^+]_o$ was 425 mM. Initially, the ASW was HCO_3-free. At the time indicated by point *a*, dialysis is begun with a dialysis fluid (DF) buffered to pH 6.5 that contained no Na^+, but 400 mM Cl^-. The absence of intracellular Na^+ should prevent reversal of the pH_i-regulating mechanism. The presence of 400 mM intracellular Cl^- should nearly saturate the transporter, which has an apparent K_m for Cl^- of ~84 mM (Boron and Russell, 1983). Finally, the low pH of the DF causes pH_i to progressively fall (segment *ab*), thereby stimulating the pH_i-regulating mechanism. When dialysis is halted at point *b*, pH_i drifts upwards very slowly and then stabilizes (*bc*). Switching the ASW to one containing 12 mM HCO_3^-/0.5% CO_2 produces an immediate fall in pH_i (*cd*) due to the influx of the CO_2 and the resultant production of H^+ and HCO_3^-. This is followed by a sustained pH_i recovery (*de*) that reflects the activity of the axon's pH_i-regulating system. The rate of pH_i recovery corresponds to a J_H of 10.8 pmol cm^{-2} s^{-1}, after correction (see

Boron, 1985) for the slight pH_i drifts during the initial HCO_3-free baseline period (*bc*) and a final baseline period in SITS (4-acetamido-4′-isothiocyanostilbene-2,2′-disulfate) (*gh*).

The addition of 1 mM DNDS to the ASW (*ef*) reduces the rate of pH_i recovery (predicted J_H = 1.7 pmol cm^{-2} s^{-1}). This inhibitory effect of DNDS is fully reversible, as evidenced by the increase in the pH_i recovery rate when the DNDS is removed (*fg*). The rate of alkalinization during this period corresponds to a J_H of

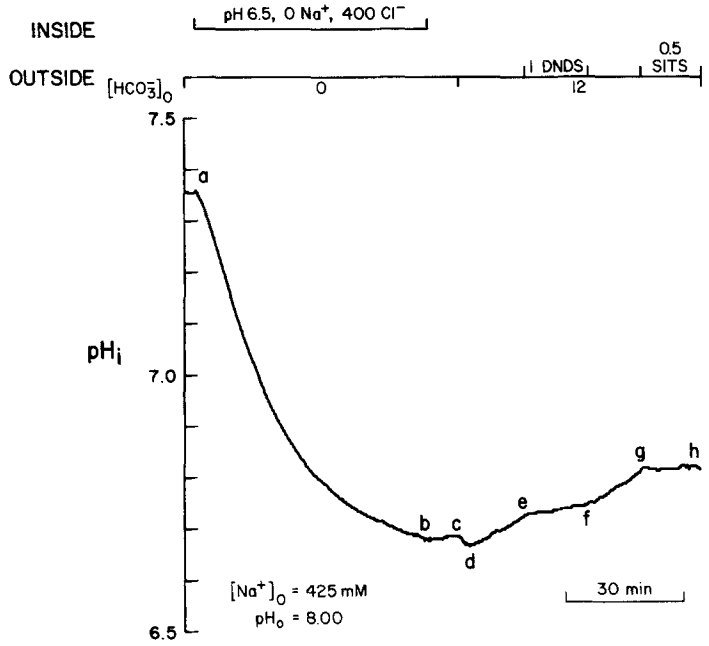

FIGURE 1. Effect of DNDS on acid extrusion. At point *a*, the flow of dialysis fluid (DF) was begun, leading to a gradual fall of intracellular pH (pH_i). Because $[Na^+]_{DF} = 0$ and $[Cl^-]_{DF}$ = 400 mM, there was presumably also a rise in axoplasmic $[Na^+]$ and a fall in $[Cl^-]$. At point *b*, dialysis was halted, so that axoplasmic processes determined the subsequent course of pH_i. After a slight rise, pH_i stabilized at *c* (initial baseline), and failed to recover in the absence of HCO_3^-. The introduction of HCO_3^- lead to the rapid pH_i recovery (*de*) that was reversibly inhibited by 1 mM DNDS (*ef*). Application of 0.5 mM SITS to the artificial seawater (ASW) blocked further pH_i recovery (*gh*).

12.8 pmol cm^{-2} s^{-1}, very similar to the value during *de*, before the addition of DNDS. The observation that J_H in squid axons is relatively insensitive to pH_i changes in the range 6.6–6.9 (e.g., compare *de* and *fg*) has been made previously (Boron, 1985), and is consistent with the observation that J_H increases only about twofold as pH_i is increased from ~6.7 to ~7.3. If the J_H values in the initial (*de*) and final (*fg*) control periods are averaged, the inhibition by DNDS in this experiment amounts to ~86%. Finally, application of 0.5 mM SITS, known to block the axon's pH_i-regulating system, blocks further recovery of pH_i (*gh*). The promptness of the blockade by

SITS indicates that delays caused by mixing of the ASWs in the chamber are minimal.

In a group of similar experiments, the inhibitory effect of DNDS on acid extrusion was determined for drug concentrations between 0.1 and 2 mM under the "standard" conditions of our experiments (i.e., $[Na^+]_o$ = 425 mM, $[HCO_3^-]_o$ = 12 mM, pH_o = 8.00). A total of 40 data points were obtained, with up to three values of $[DNDS]_o$ tested in each axon. In most experiments, the blockade of acid extrusion during the final baseline period (corresponding to *gh* in Fig. 1) was achieved by nominal removal of HCO_3^-/CO_2. The data from this study are summarized in Fig. 2. The results of a nonlinear least-squares curve fit (see Methods) indicate that half-maximal inhibition was achieved at 0.31 ± 0.06 mM DNDS, with an apparent maximal inhibition of 104 ± 7%. Because the maximal inhibition by the drug was indistinguishable from 100%, these data rule out substantial contribution from rapid-equilibrium kinetic schemes (e.g., partial competitive inhibition, partial non-

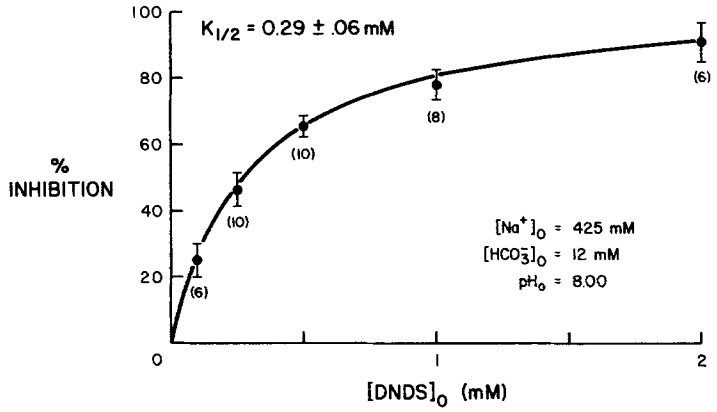

FIGURE 2. Inhibition of acid extrusion by DNDS. All data were obtained at $[Na^+]_o$ = 425 mM, nominal $[HCO_3^-]_o$ = 12 mM, and pH_o = 8.00.

competitive inhibition) in which an enzyme-substrate-inhibitor complex leads to acid extrusion, but at a lower rate than the enzyme-substrate complex. Fitting the data to the Hill equation for multiple inhibitors (Segel, 1975) yielded a coefficient of 1.08 ± 0.14 (not shown).

Effect of DNDS on the HCO_3^- Dependence of Acid Extrusion

To determine the nature of the inhibition of acid extrusion by DNDS, we studied the effect of the drug on the external-HCO_3^- dependence of acid extrusion. The experiments were similar in design to that of Fig. 1, and were always carried out at the pH_o of 8.00 and a $[Na^+]_o$ of 425 mM. A nonlinear least-squares curve fit of the data obtained in the absence of DNDS yielded a J_{max} of 20.5 pmol cm^{-2} s^{-1}, and a $K_m(HCO_3^-)$ of 2.6 mM, as previously reported (Boron, 1985). Similar individual curve fits (see Methods) were also performed on data obtained at $[DNDS]_o$ levels of 0.1 and 0.25 mM. As is evident from Fig. 3 and Table I, J_{max} was not significantly

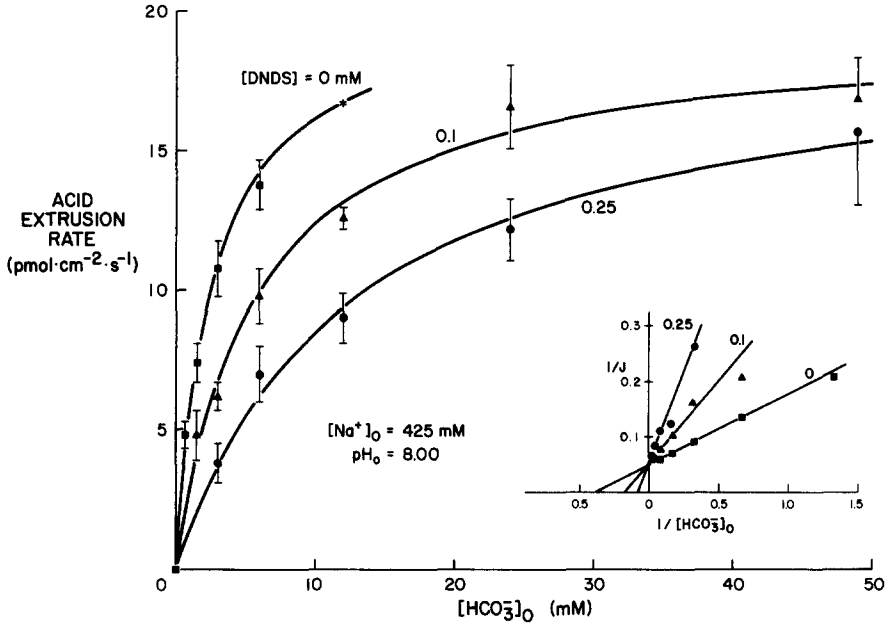

FIGURE 3. Effect of DNDS on the external HCO_3^- dependence of acid extrusion. All data were obtained at $[Na^+]_o$ = 425 mM and pH_o = 8.00. $[DNDS]_o$ was either 0, 0.1, or 0.25 mM. The inset is a replot of the data in double reciprocal form.

affected by raising $[DNDS]_o$, whereas $K_m(HCO_3^-)$ increased substantially, rising to 5.7 and 12.7 mM at $[DNDS]_o$ levels of 0.1 and 0.25 mM, respectively. Thus, DNDS behaves as a competitive inhibitor with respect to extracellular HCO_3^-.

The apparent inhibitory constant for DNDS (K_i) could be determined by simultaneously fitting the 106 normalized data points of Fig. 3 (also summarized in Table I) to an equation of the form of Eq. 2 (see Methods), which forces the fitted curve through the point describing our "standard" conditions (i.e., $[HCO_3^-]_o$ = 12 mM, $[Na^+]_o$ = 425 mM, $[DNDS]_o$ = 0 mM, and J_H = 16.8 pmol cm^{-2} s^{-1}). The fitting procedure independently determines only $K_m(HCO_3^-)$ and K_i(DNDS), with the J_{max} computed from the best-fit values of the apparent K_m and K_i using Eq. 3 (see Methods).

TABLE I

Dependences of Acid Extrusion Rate on $[HCO_3^-]_o$ at Three Levels of $[DNDS]_o$*

$[Na^+]$	$[DNDS]_o$	n	Fit*	Apparent $K_m(HCO_3^-)$	Apparent J_{max}
mM	*mM*			*mM*	*pmol cm⁻² s⁻¹*
425	0	31	2	2.6 ± 0.3	20.5 ± 2.2
425	0.1	40	1	5.7 ± 1.3	19.5 ± 1.3
425	0.25	35	1	12.7 ± 4.3	19.3 ± 2.5

*Nonlinear least-squares curve fits, as described in methods, were individually performed on each of the three sets of data points. Type 1 fit: standard Michaelis-Menten equation. Type 2 fit: forced through a standard point ($[Na^+]_o$ = 425 mM, $[HCO_3^-]_o$ = 12 mM, pH_o = 8.00, and $[DNDS]_o$ = 0 mM). n is the number of points fitted. The data at $[DNDS]_o$ = 0 mM were previously reported (Boron, 1985).

TABLE II

*Kinetic Parameters Obtained from Simultaneous Fits of Data**

Substrate varied	$[HCO_3^-]_o$	$[Na^+]_o$	n	Apparent $K_m(HCO_3^-)$	Apparent $K_m(Na^+)$	Apparent K_i(DNDS)	Apparent J_{max}
	mM	*mM*		*mM*	*mM*	*μM*	*pmol cm^{-2} s^{-1}*
HCO_3^-	—	425	106	2.4 ± 0.4	—	55 ± 9	20.1
Na^+	12	—	59	—	70.1 ± 10.5	53 ± 13	19.5
Na^+	48	—	118	—	19.5 ± 4.0	64 ± 16	19.9

*The fits in line 1 were performed on the data of Table I, those in line 2, on the data of Table III (top), and those in line 3, on the data of Table III (bottom).

The results of this fit, summarized in Table II, are a $K_m(HCO_3^-)$ of 2.4 ± 0.4 mM, and a K_i(DNDS) of 55 ± 9 μM. The J_{max} computed from these values is 20.1 pmol cm^{-2} s^{-1}.

Effect of DNDS on the Na^+ Dependence of Acid Extrusion

The effect of DNDS on the extracellular Na^+ dependence of acid extrusion was determined at two levels of $[HCO_3^-]_o$, 12 and 48 mM, always at a pH_o of 8.00. Data obtained at a $[HCO_3^-]_o$ of 12 mM are summarized in Fig. 4 and in the top portion of Table III. The results of an individual curve fit indicate that in the absence of DNDS, J_{max} is 19.7 pmol cm^{-2} s^{-1} and $K_m(Na^+)$ is 71 mM, as reported in a previous study (Boron, 1985). Raising $[DNDS]_o$ to 0.1 mM has no substantial effect on J_{max},

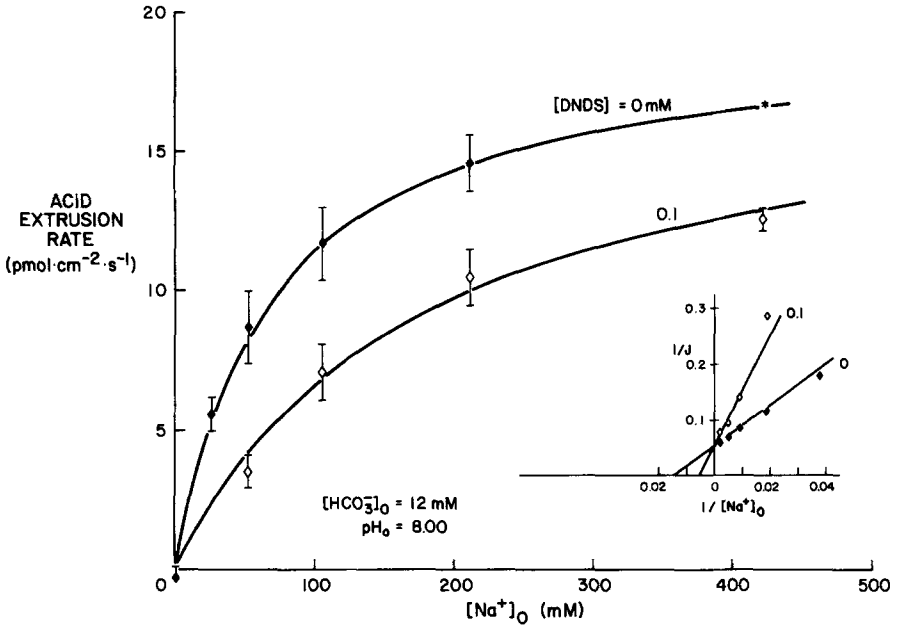

FIGURE 4. Effect of DNDS on the external Na^+ dependence of acid extrusion. All data were obtained at nominal $[HCO_3^-]$ = 12 mM and pH_o = 8.00. $[DNDS]_o$ was either 0 or 0.1 mM. The inset is a replot of the data in double reciprocal form.

but increases $K_m(Na^+)$ to 179 mM. This is consistent with simple competitive inhibition of DNDS with respect to Na^+. It would have been desirable to extend this study to a $[DNDS]_o$ of 0.25 mM. However, at a $[HCO_3^-]_o$ of only 12 mM, the likely $K_m(Na^+)$ in 0.25 mM DNDS would have approached the maximal $[Na^+]_o$ we could have achieved under isotonic conditions (i.e., 425 mM). Because it would have been difficult to obtain J_{max} and $K_m(Na^+)$ values from curve fits of data obtained under these conditions, we decided to forgo further experiments at a $[HCO_3^-]_o$ of 12 mM.

The two series of data obtained at a $[HCO_3^-]_o$ of 12 mM (i.e., $[DNDS]_o$ = 0 or 0.1 mM) can be used to obtain an apparent inhibitory constant for DNDS. Our approach was to simultaneously fit all 59 data points obtained with a $[HCO_3^-]_o$ of 12 mM (see Fig. 4 and the top of Table III) to an equation of the form of Eq. 2 (see Methods), which forces the fitted curve through the "standard" point ($[HCO_3^-]_o$ = 12 mM, $[Na^+]$ = 425 mM, $[DNDS]_o$ = 0, and J_H = 16.8 pmol cm^{-2} s^{-1}). The results of this calculation, summarized in line 2 of Table II, are a $K_m(Na^+)$ of

TABLE III

Dependence of Acid Extrusion on $[Na^+]_o$ at Three Levels of $[DNDS]_o$*

$[HCO_3^-]_o$	$[DNDS]_o$	n	Fit*	Apparent $K_m(Na^+)$	Apparent J_{max}
mM	*mM*			*mM*	*pmol cm^{-2} s^{-1}*
12	0	35	2	71 ± 12	19.7
12	0.1	24	1	179 ± 54	18.5 ± 2.4
48	0	42	1	22 ± 6	20.8 ± 1.8
48	0.1	43	1	45 ± 12	20.3 ± 1.8
48	0.25	33	1	90 ± 31	18.6 ± 2.4

*Nonlinear least-squares curve fits, as described in Methods, were individually performed on each of the three sets of data points. Type 1 fit: standard Michaelis-Menten equation. Type 2 fit: forced through a standard point ($[HCO_3^-]_o$ = 12 mM, $[Na^+]_o$ = 425 mM, $[DNDS]_o$ = 0 mM, and J_H = 16.8 pmol cm^{-2} s^{-1}). n is the number of points fitted. The data at $[HCO_3^-]_o$ = 12 mM/$[DNDS]_o$ = 0 mM were previously reported (Boron, 1985).

70 ± 10 mM, and a K_i(DNDS) of 53 ± 13 μM. The J_{max} computed from these values is 19.5 pmol cm^{-2} s^{-1}.

Because it was not feasible to examine the effect of 0.25 mM DNDS on the $[Na^+]_o$ dependence of J_H when $[HCO_3^-]_o$ was only 12 mM, (see above) we performed additional experiments at a $[HCO_3^-]_o$ of 48 mM. Inasmuch as increasing $[HCO_3^-]_o$ in the range of 3–12 mM causes a reciprocal change in the apparent K_m for Na^+ (Boron, 1985), we anticipated that increasing $[HCO_3^-]_o$ to 48 mM would cause $K_m(Na^+)$ to fall. The ion-pair model predicts that $K_m(Na^+)$ should decline to ~20 mM in the absence of DNDS. This would have the advantage of allowing us to examine the effect of relatively high doses of DNDS (i.e., 0.25 mM), while $K_m(Na^+)$ is kept substantially below the maximal obtainable $[Na^+]_o$. The results of this series of experiments are summarized in Fig. 5 and the lower portion of Table III. In the absence of DNDS, J_{max} was 20.8 pmol cm^{-2} s^{-1}, and the $K_m(Na^+)$ was 22 mM. Comparing these values to those obtained in the absence of DNDS in 12 mM HCO_3^-, we see that raising $[HCO_3^-]_o$ to 48 mM has a minimal effect on J_{max}, but causes a substantial reduction in $K_m(Na^+)$. Thus, this result agrees with the prediction of the ion-pair

model. With $[HCO_3^-]_o$ at 48 mM, raising $[DNDS]_o$ to 0.1 and 0.25 mM has a minimal effect on J_{max}, but causes $K_m(Na^+)$ to increase to 45 and 90 mM, respectively.

The 118 data points obtained at a $[HCO_3^-]_o$ of 48 mM can be simultaneously fitted to an equation of the form of Eq. 2, as described above. The results of such a calculation, summarized on line 3 of Table II, are a $K_m(Na^+)$ of 19.5 ± 4.0 mM, and apparent K_i(DNDS) of 64 ± 16 μM.

The Na^+ dependence of J_H, both 12 mM and 48 mM HCO_3^-, indicates that DNDS has almost no effect on the apparent J_{max}, but greatly increases the apparent K_m for Na^+. These observations are consistent with simple competitive inhibition between DNDS and Na^+. It should be noted that the K_i(DNDS) and J_{max} values generated by

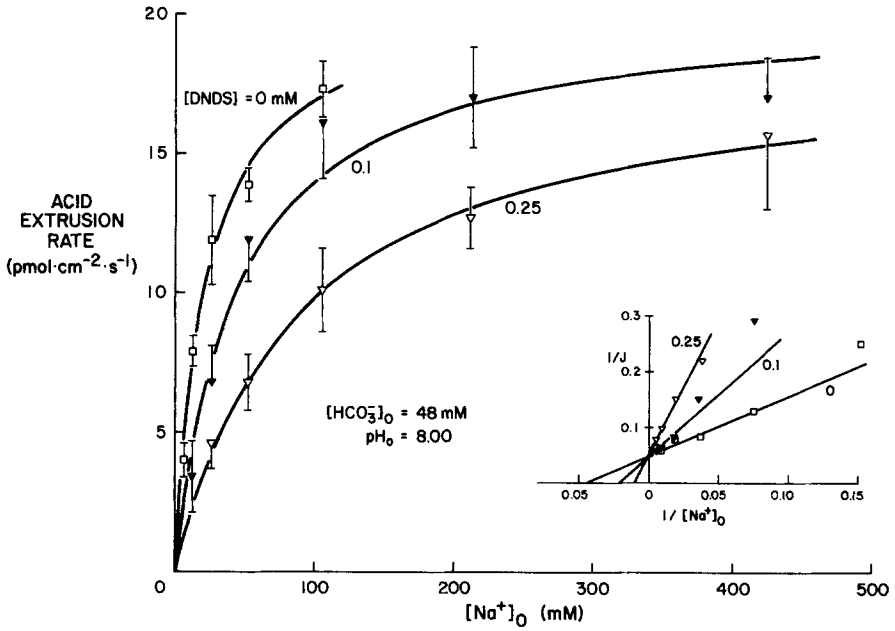

FIGURE 5. Effect of DNDS on the external Na^+ dependence of acid extrusion. All data were obtained at nominal $[HCO_3^-]_o$ = 48 mM and pH_o = 8.00. $[DNDS]_o$ was either 0, 0.1, or 0.25 mM. The inset is a replot of the data in double reciprocal form.

the three simultaneous curve fits were very similar (see Table II); whether (*a*) $[HCO_3^-]_o$ was varied at a $[Na^+]_o$ of 425 mM, or (*b*) $[Na^+]_o$ was varied at a $[HCO_3^-]_o$ of 12 mM, or whether (*c*) $[Na^+]_o$ was varied at a $[HCO_3^-]_o$ of 48 mM, the apparent J_{max} differed only slightly from 20 pmol cm^{-2} s^{-1}, and the apparent K_i(DNDS) ranged from 53 to 64 μM.

DISCUSSION

Inhibition of Acid Extrusion by DNDS

Although disulfonic stilbene derivatives such as SITS and DIDS (4,4′-diisothiocyanostilbene-2,2′-disulfonate) are known to inhibit several anion transport systems,

their effects were studied first on the erythrocyte band 3 protein, which mediates Cl-HCO_3 exchange (Cabantchik et al., 1978). The interaction of SITS and DIDS with the erythrocyte Cl-HCO_3 exchanger occurs in two steps (Cabantchik and Rothstein, 1972). The first is a rapid and reversible binding, and the second is a slower covalent reaction between the isothiocyano group on the stilbene and an amino group on the transporter. Inasmuch as DNDS lacks the isothiocyano group, it can only participate in the first step, which is probably an ionic interaction between the negatively charged sulfonate groups on the DNDS and positively charged regions of the Cl-HCO_3 exchanger. DNDS competitively inhibits the sulfate equilibrium exchange mediated by the Cl-HCO_3 exchanger, with an inhibitory constant of ~0.45 mM, and a Hill coefficient of unity (Barzilay and Cabantchik, 1979). Fröhlich (1982) has shown that the DNDS binding capacity of erythrocytes is about one million/cell, approximately the same as for disulfonic stilbenes possessing isothiocyano groups. This binding of DNDS, which occurs with a binding constant of ~84 nM, is competitively inhibited by external Cl^- with a Cl^- inhibitory constant of ~6 mM. Furthermore, DNDS competitively inhibits external Cl^-–stimulated Cl^- efflux with an inhibitory constant of 90 nM. Thus, the data point to an interaction between DNDS and a single class of sites on the erythrocyte, and simple competitive inhibition by DNDS of anion binding.

It is known that, qualitatively at least, the disulfonic stilbene derivatives and certain other compounds containing isothiocyano groups behave toward the Na^+-dependent Cl-HCO_3 exchanger in much the same way as they do toward the erythrocyte Cl-HCO_3 exchanger. Thus, DIDS and SITS block the acid extrusion (Russell and Boron, 1976; Thomas, 1976), Cl^- fluxes (Russell and Boron, 1976), intracellular Na^+ activity changes (Thomas, 1977), and Na^+ fluxes (Boron and Russell, 1983) mediated by the Na^+-dependent Cl-HCO_3 exchangers of squid axons, snail neurons, and barnacle muscle. Moreover, DNDS reversibly inhibits acid extrusion mediated by the Na^+-dependent Cl-HCO_3 exchanger of barnacle muscle (Boron, 1977) and the squid axon (Boron and Russell, 1983).

In light of the similar effects of the disulfonic stilbenes on erythrocyte Cl-HCO_3 exchangers and invertebrate pH_i-regulating mechanisms, we might anticipate that the inhibition by DNDS of acid extrusion in the squid axon might be competitive with respect to anions and have a Hill coefficient of unity. These expectations have been confirmed by the present study. We found that at pH_o 8.00 and in the presence of 12 mM HCO_3^- and 425 mM Na^+, DNDS reversibly and progressively inhibited acid extrusion. The apparent K_i (DNDS) under these conditions was ~0.3 mM, the best-fit maximal inhibition was 104%, and the best-fit Hill coefficient for multiple inhibitors was 1.08. Furthermore, in studies in which we examined the effect of DNDS on the $[HCO_3^-]_o$ dependence of acid extrusion, we found that DNDS behaved as a simple competitor, with an inhibitory constant of ~55 μM. The three-order-of-magnitude discrepancy between the K_i (DNDS) values in our squid-axon study and Fröhlich's erythrocyte study could simply reflect fundamental differences between Na^+-dependent and Na^+-independent Cl-HCO_3 exchangers. It should be pointed out, however, that Fröhlich (1982) found that the apparent K_i (DNDS) is linearly related to $[Cl^-]_o$, at least in the range 0–12 mM. Although the K_i (DNDS) for the erythrocyte Cl-HCO_3 exchanger was 84 nM at $[Cl^-]_o$ = 0, it rose to ~240 nM at $[Cl^-]_o$ = 12 mM. Inasmuch as our experiments were conducted at a $[Cl^-]_o$ of

~535 mM, it is possible that a large portion of the apparent discrepancy reflects the high levels of a potentially competing anion (i.e., Cl^-) in our seawaters.

Although the evidence we obtained for apparent competition between DNDS and HCO_3^- is not surprising, that for competition between DNDS and Na^+ may not have been anticipated. In the classical model of competitive inhibition, the substrate and inhibitor bind to the same site, and are structurally similar. Although it is easy to interpret the competition between DNDS (a divalent anion) and HCO_3^- in terms of such a model, the apparent competition between DNDS and Na^+ cannot be accounted for. Thus, if DNDS does behave as a classic competitive inhibitor, the most straightforward explanation for the competition between DNDS and Na^+ is the $NaCO_3^-$ ion-pair model (see below).

However, DNDS need not be structurally similar to Na^+ in order to appear to be a competitive inhibitor. Other possibilities (see Segel, 1975) are that (*a*) the binding of DNDS and Na^+ are mutually exclusive for steric reasons, (*b*) the binding sites for DNDS and Na^+ are distinct but overlapping, and (*c*) the binding of DNDS induces a conformational change in the transporter that prevents binding of Na^+.

Analysis of Kinetic Models

Inasmuch as our observation that DNDS is apparently competitive with respect to both HCO_3^- and Na^+ does not allow us to rule out, a priori, models in which Na^+ and HCO_3^- (or $CO_3^=$) separately bind to the transporter, we examined the predictions of four rapid-equilibrium models: (*a*) binding of the $NaCO_3^-$ ion pair, (*b*) random binding of Na^+ and HCO_3^- (or $CO_3^=$), (*c*) ordered binding of Na^+ and then HCO_3^- (or $CO_3^=$), and (*d*) ordered binding of HCO_3^- (or $CO_3^=$) and then Na^+. The predictions for the binding of a single HCO_3^- and a single $CO_3^=$ are the same, provided the data are all gathered at the same external pH. Furthermore, these models are applicable to schemes involving the binding of two HCO_3^-, provided the affinities of the two HCO_3^--binding sites are sufficiently different from one another.

A kinetic analysis of these models is detailed in Appendix 2, and summarized below and in Tables IV and VI. The goal of this analysis, and indeed the entire study, was to attempt to rule out the ion-pair model. This is straightforward if the data conflict with the kinetic predictions of the ion-pair model. However, as shown below, the present DNDS data, as well as earlier data dealing with the interaction between Na^+ and HCO_3^- in the absence of DNDS (Boron, 1985), are nicely fitted by the ion-pair model. This raises an unavoidable dilemma that flows from the mathematical descriptions of the other kinetic models (see Appendix 2): the predictions of the other kinetic models reduce to those of the ion-pair model as their kinetic parameters approach extreme values. Thus, insofar as any data fit the ion-pair model, they can also be fitted by the other models. Although we cannot rule out these other models, we can place severe restrictions on their permissible kinetic parameters.

Ion-Pair Model

We have analyzed the ion-pair model (see Appendix 2 for details) for each of the eight groups of data described in Results (series 1–8), as well as the four additional groups of data (series A–D) described previously (Boron, 1985). On line 1 of Table

TABLE IV

*Comparison of Observed Kinetic Parameters and Those Predicted by Rapid-Equilibrium Kinetic Models**

	A. $K_m(HCO_3^-)$, *mM*				
Series:	1	2	3	A	B
[Na]:	425	425	425	212	106
[HCO_3]:	—	—	—	—	—
[DNDS]:	0	0.1	0.25	0	0
1) Observed	2.6 ± 0.3	5.7 ± 1.3	12.7 ± 4.3	5.4 ± 1.0	9.7 ± 2.1
2) Ion-pair	2.2	6.0	11.7	4.5	8.9
3) Random	3.2	7.3	13.5	4.7	7.3
4) Na^+, HCO_3^-	3.4	7.8	14.4	5.4	9.5
5) HCO_3^-, Na^+	1.6	5.1	10.2	3.2	6.0
	B. $J_{max}(HCO_3^-)$, *pmol* cm^{-2} s^{-1}				
Series:	1	2	3	A	B
[Na]:	425	425	425	212	106
[HCO_3]:	—	—	—	—	—
[DNDS]:	0	0.1	0.25	0	0
1) Observed	20.5 ± 2.2	19.5 ± 1.3	19.3 ± 2.5	18.7 ± 1.2	19.2 ± 1.5
2) Ion-pair	19.8	19.8	19.8	19.8	19.8
3) Random	21.3	21.3	21.3	20.7	19.6
4) Na^+, HCO_3^-	21.4	21.4	21.4	21.4	21.4
5) HCO_3^-, Na^+	19.1	19.1	19.1	18.5	17.5

C. $K_m(Na^+)$, *mM*

Series:	4	5	6	7	8	C	D
[Na]:	—	—	—	—	—	—	—
[HCO_3]:	12	12	48	48	48	6	3
[DNDS]:	0	0.1	0	0.1	0.25	0	0
1) Observed	71 ± 12	179 ± 54	22 ± 6	45 ± 12	90 ± 31	174 ± 45	261 ± 102
2) Ion-pair	79	213	20	53	104	158	315
3) Random	60	190	25	62	116	96	149
4) Na^+, HCO_3^-	65	205	18	56	113	118	200
5) HCO_3^-, Na^+	73	197	28	59	106	132	252

D. $J_{max}(Na^+)$, *pmol* cm^{-2} s^{-1}

Series:	4	5	6	7	8	C	D
[Na]:	—	—	—	—	—	—	—
[HCO_3]:	12	12	48	48	48	6	3
[DNDS]:	0	0.1	0	0.1	0.25	0	0
1) Observed	19.7 ± 3.4	18.5 ± 2.4	20.8 ± 1.8	20.3 ± 1.8	18.6 ± 2.4	18.4 ± 2.0	15.4 ± 3.2
2) Ion-pair	19.8	19.8	19.8	19.8	19.8	19.8	19.8
3) Random	19.1	19.1	21.1	21.1	21.1	17.0	13.8
4) Na^+, HCO_3^-	19.3	19.3	20.9	20.9	20.9	17.6	14.9
5) HCO_3^-, Na^+	19.6	19.6	19.6	19.6	19.6	19.6	19.6

*For each of four kinetic parameters, observed values are presented for several experimental conditions. Also presented are values predicted for four models: ion pair, random binding, ordered binding of Na^+ then HCO_3^-, and ordered binding of HCO_3^- then Na^+. These predicted values were computed from the best-fit values in Table VI.

IV are the observed values for each of the experimentally determined kinetic parameters: (*A*) K_m (HCO_3^-), (*B*) J_{max}(HCO_3^-), (*C*) K_m(Na^+) and (*D*) J_{max}(Na^+). On line 2, are the corresponding values predicted from a least-squares fit of the ion-pair model to our data. (See line 1 of Table VI for the best-fit parameters.) As can be seen, the fit is excellent, with predicted values always falling well within two standard deviations of the observed K_m's and J_{max}'s. Based on the sum of squares of residuals, the ion-pair model fits the data marginally better than any of the others.

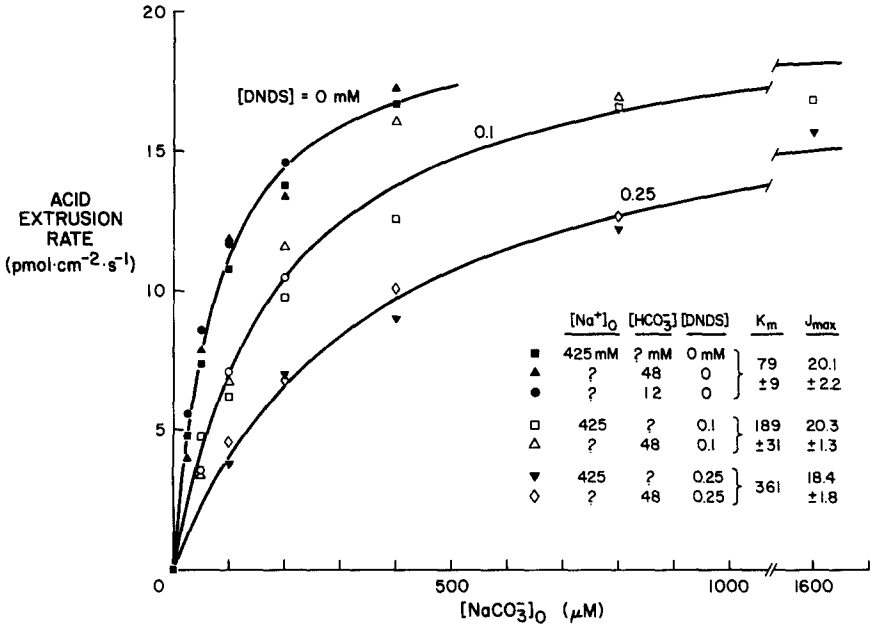

FIGURE 6. Dependence of acid-extrusion rate on the calculated $[NaCO_3^-]_o$ at DNDS levels of 0, 0.1, and 0.25 mM. All 348 J_H vs. $[Na^+]_o$ or J_H vs. $[HCO_3^-]_o$ data points reported in this paper are replotted as J_H vs. $[NaCO_3^-]_o$. The $[NaCO_3^-]_o$ values are nominal, and were calculated as described in footnote 1. The curves drawn through the points are the result of a simultaneous fit of all of the data to an equation of the form of Eq. 1.

For the ion-pair model to be viable, all data obtained at a single $[DNDS]_o$ must fall along the same J_H vs. $[NaCO_3^-]_o$ curve, regardless of $[HCO_3^-]_o$ or $[Na^+]_o$. In Fig. 6 we have plotted J_H as a function of the calculated[1] $[NaCO_3^-]_o$ for $[DNDS]_o$ levels of 0, 0.1, and 0.25 mM. The curves drawn through the points are the result of a simultaneous fit of all 348 data points to an equation of the form of Eq. 1 (Table V, line 1). As can be seen from the three curves, as well as the individual fits of the data to the Michaelis-Menten equation (Table V, lines 2–4), J_{max} is not significantly affected by changes in $[DNDS]_o$, whereas K_m($NaCO_3^-$) increases with increasing levels of the

[1] As discussed in Appendix 1, $[NaCO_3^-]_o = ([Na^+]_o[HCO_3^-]_o)/(\gamma 10^{-pH_o})$. We computed $[NaCO_3^-]_o$ from the nominal $[HCO_3^-]_o$ and $[Na^+]_o$, assuming that $\gamma = 1.7 \times 10^6$ M (Garrells et al., 1961), and that $pH_o = 8.00$.

TABLE V

Summary of Data in Terms of Calculated $[NaCO_3^-]_o$*

$[DNDS]_o$	n	Fit*	Apparent $K_m(NaCO_3^-)$	Apparent K_i(DNDS)	Apparent J_{max}
mM			*μM*	*μM*	*pmol cm^{-2} s^{-1}*
All	348	1	56 ± 5	59 ± 6	19.9 ± 0.6
0	193	2	59 ± 6	—	20.3 ± 0.8
0.1	93	1	132 ± 22	—	19.4 ± 1.2
0.25	62	1	270 ± 67	—	18.4 ± 1.8

*Nonlinear least-squares curve fits, as described in Methods, were individually performed on each of the three sets of data points. Type 1 fit: standard Michaelis-Menten equation. Type 2 fit: forced through a standard point ($[HCO_3^-]_o$ = 12 mM, $[Na^+]_o$ = 425 mM, $[DNDS]_o$ = 0 mM, and J_H = 16.8 pmol cm^{-2} s^{-1}). n is the number of points fitted. The data at $[DNDS]_o$ = 0 mM were previously reported (Boron, 1985).

inhibitor. Thus, this analysis is also consistent with the hypothesis that DNDS competes with the $NaCO_3^-$ ion pair.

Random Binding of Na^+ and HCO_3^-

An analysis of the rapid-equilibrium model in which Na^+ and HCO_3^- bind randomly to the carrier, each competing with DNDS, is provided in Appendix 2. The predicted apparent K_m and J_{max} values are summarized in line 3 of Table IV; these were computed from the best-fit parameters (see Table VI, line 2). As noted in Appendix 2, the predictions of the random-binding model reduce to those of the ion-pair model at extreme values for the kinetic parameters. Indeed, the overall fit of the random-binding model to the 348 data points produced a sum of squares of residuals that was only ~2.6% higher than that of the ion-pair model.

Ordered Binding of Na^+ and HCO_3^-

Appendix 2 also contains an analysis of a rapid-equilibrium model in which first Na^+ and then HCO_3^- bind to the carrier, with DNDS competing with Na^+. The predicted apparent K_m and J_{max} values, computed from these best-fit parameters (see Table VI, line 3), are summarized in line 4 of Table IV. As for the predictions of the random-binding model, those of the ordered Na^+-then-HCO_3^- model reduce to those of the ion-pair model for extreme values of the kinetic parameters. Indeed, the overall fit

TABLE VI

*Summary of Best-Fit Values for Rapid-Equilibrium Kinetic Models**

Model	α	K_{NaCO_3}	K_{Na}	K_{HCO_3}	K_i	J_{max}	SSR
		μM	*mM*	*mM*	*μM*	*pmol cm^{-2} s^{-1}*	
Ion pair	—	55.6	—	—	58.7	19.9	9.09
Random	0.0321	—	385	4.4	37.4	21.9	9.33
Na^+, HCO_3^-	—	—	653	1.32	46.0	21.4	9.29
HCO_3^-, Na^+	—	—	12.8	56.0	37.4	19.6	9.96

*The results of nonlinear least-squares curve fits are presented for four kinetic models: ion pair, random binding, ordered binding of Na^+ then HCO_3^-, and ordered binding of HCO_3^- then Na^+. *SSR* is the sum of squares of residuals. See Appendix 2 for details.

of this random-binding model to the 348 data points produced a sum of squares of residuals that was only ~2.2% higher than that of the ion-pair model.

Ordered Binding of HCO_3^- then Na^+

The final kinetic analysis in Appendix 2 is of a rapid-equilibrium model in which first HCO_3^- and then Na^+ bind to the carrier, with DNDS competing with HCO_3^-. The predicted apparent K_m and J_{max} values, computed from these best-fit parameters (see Table VI, line 4), are summarized in line 5 of Table IV. As for the predictions of the random-binding and ordered Na^+-then-HCO_3^- models, those of the ordered HCO_3^--then-Na^+ model reduce to those of the ion-pair model for extreme values of the kinetic parameters. The overall fit of this random-binding model to the 348 data points produced a sum of squares of residuals that was only ~10% higher than that of the ion-pair model.

Conclusions

The disulfonic stilbene derivative DNDS appears to be a competitive inhibitor of acid extrusion, with respect to both HCO_3^- and Na^+. The data are entirely consistent with the $NaCO_3^-$ ion-pair model. Indeed, this model provides the best fit to the data, and is probably the most straightforward. However, three other rapid-equilibrium kinetic models (random binding, ordered binding of Na^+ then HCO_3^-, and ordered binding of HCO_3^- then Na^+) also produce reasonable fits of the data, and therefore cannot be ruled out.

Two points deserve emphasis. First, given the excellent fit provided by the ion-pair model, it was unavoidable that the other models should also fit the data. As shown in Appendix 2, the predictions of the other models reduce to those of the ion-pair model for extreme values of the kinetic parameters. This result can be reached intuitively: The ion-pair model states that Na^+ and $CO_3^=$ first complex with one another before binding to the carrier. However, this should be indistinguishable from the case in which the binding of Na^+ makes the carrier's affinity for $CO_3^=$ infinitely high, and vice versa.

Second, given the excellent fit of the ion-pair model, we would not have been able to distinguish among the models even if we had employed a broader range of values of $[HCO_3^-]_o$, $[Na^+]_o$, and $[DNDS]_o$. This is because the predictions of all of the models reduce to those of the ion-pair model, regardless of substrate or inhibitor concentration. In fact, the range of values examined in this and the preceding study was as broad as practicable. Had we used lower values of $[Na^+]_o$, we would have had to have used higher values of $[HCO_3^-]_o$ to achieve saturation. However, raising $[HCO_3^-]_o$ would require raising $[CO_2]_o$ to keep pH_o constant. This, in turn, would have raised $[HCO_3^-]_i$ and, thus, the total intracellular buffering power. Thus, rates of pH_i change would have been extremely low. Had we used lower values of $[HCO_3^-]_o$, we would have had to have used higher values of $[Na^+]_o$ to achieve saturation. However, we could not raise $[Na^+]_o$ above ~500 mM without making the solutions hypertonic.

In summary, the data are fitted well by the ion-pair model. Although we cannot rule out three other rapid-equilibrium models, we can place severe restrictions on the allowable kinetic parameters for each of them.

APPENDIX I

Calculation of Concentrations of HCO_3^--derived Species after HCO_3^- Is Added to a Solution

To perform the kinetic analyses presented in the Discussion, one must know the concentration of HCO_3^-, or of related species (e.g., $NaCO_3^-$). However, the relationship between added HCO_3^- and $[HCO_3^-]$ is complex. For example, we have found that adding 12 mM $KHCO_3$ to seawater, initially buffered to pH 8.00 with 30 mM EPPS, causes a paradoxical fall in pH to ~7.97. This observation implies that less of the added HCO_3^- participates in the reaction $HCO_3^- + H^+ \rightarrow H_2CO_3$ than in the reaction $HCO_3^- \rightarrow CO_3^= + H^+$. We suspected that the latter reaction is promoted by the complexation of $CO_3^=$ with various cations to form ion pairs. Thus, the added HCO_3^- ought to be distributed in several pools, including HCO_3^- and several carbonates (e.g., $CO_3^=$, $NaCO_3^-$, $MgCO_3$, and $CaCO_3$). To the extent that carbonate formation occurs, the assumption that $[HCO_3^-]$ equals the added HCO_3^- will be in error. Because this issue is crucial for the present study, as well as a forthcoming one in which we examine the effects of extracellular pH changes on acid-extrusion rates, we analyzed the chemistry of HCO_3^- in solutions containing cations that complex with $CO_3^=$. Our analysis shows that carbonate formation causes $[HCO_3^-]$ to be only ~10% lower than the added HCO_3^- at pH_o 8.00 (i.e., the conditions of the present experiments), and that the error increases with increasing pH_o. The analysis is relevant for any HCO_3^--containing solution at high pH.

HCO_3^- added to an aqueous solution (in an amount $[HCO_3^-]^\circ$) has one of three general fates: (*a*) the greatest portion remains HCO_3^-, (*b*) a small amount (x) of the HCO_3^- combines with H^+ to yield CO_2, and (*c*) a small amount (y) of the HCO_3^- dissociates into H^+ and $CO_3^=$. The flux (x) of HCO_3^--derived carbon atoms through pathway (*b*) increases if the CO_2 formed leaves solution and enters the atmosphere, whereas the flux (y) through pathway (*c*) will be increased if the $CO_3^=$ formed is consumed by the formation of $CO_3^=$-containing ion pairs. The reactions can be summarized as follows:

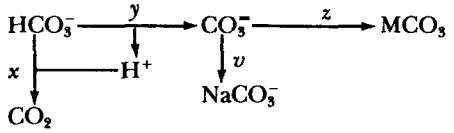

Scheme A1

where x, y, z, and v are the fluxes of HCO_3^--derived carbon atoms through the indicated reactions. M is a divalent cation (e.g., Ca^{++} or Mg^{++}). At equilibrium, when there is no net flux through any of the reactions,

$$[HCO_3^-]' = [HCO_3^-]^\circ - x - y \tag{A1}$$

$$[CO_3^=]' = y - z - v \tag{A2}$$

$$[MCO_3]' = z \tag{A3}$$

$$[NaCO_3^-]' = v \tag{A4}$$

$$[CO_2]' = x \tag{A5}$$

$$pH' = pH^\circ + (x - y)/\beta \tag{A6}$$

where the single primes following the parameter designations indicate the values pertaining after equilibrium is established. pH° is the pH prevailing before the addition of the amount

of $[HCO_3^-]^\circ$ of HCO_3^-, and β is the non-CO_2 buffering power of the solution. The following equations describe the four equilibria that are simultaneously established:

$$pH' = pK_1 + \log \frac{[HCO_3^-]'}{[CO_2]'} \quad \text{or} \quad 10^{(pH'-pK_1)} = \frac{[HCO_3^-]^\circ - x - y}{x} \tag{A7}$$

$$pH' = pK_2 + \log \frac{[CO_3^{=}]'}{[HCO_3^-]'} \quad \text{or} \quad 10^{(pH'-pK_2)} = \frac{y - z - v}{[HCO_3^-]^\circ - x - y} \tag{A8}$$

$$K_M = \frac{[CO_3^{=}]'[M]}{[MCO_3]'} \quad \text{or} \quad K_M = \frac{(y - z - v)[M]}{z} \tag{A9}$$

$$K_{Na} = \frac{[CO_3^{=}]'[Na]}{NaCO_3^-]'} \quad \text{or} \quad K_{Na} = \frac{(y - z - v)[Na]}{v} \tag{A10}$$

where it is assumed that [M] and $[Na^+]$ are not affected significantly by the formation of $CO_3^=$ ion pairs. Algebraic manipulations of the above equations lead to the following equation, which describes the pH obtaining at equilibrium in terms of the constants pK_1, pK_2, K_M, K_{Na}, M, Na, $[HCO_3^-]^\circ$, and pH°:

$$\beta(pH' - pH^\circ) + [HCO_3^-]^\circ \cdot \frac{P_2S[P_1 + P_1P_2(S + 1)] + P_1P_2 - (1 + P_2S)}{(1 + P_2S) \cdot [1 + P_1 + P_1P_2(S + 1)]} = 0 \tag{A11}$$

where $P_1 = 10^{(pH'-pK_1)}$, $P_2 = 10^{(pH'-pK_2)}$, and $S = ([M]/K_M + [Na]/K_{Na})$. This exponential equation is solved for pH' using a standard numerical technique. This value is then used to compute y, x, z, and v using the following equations, which are also derived by algebraically manipulating Eqs. (A7) through (A10):

$$x = [HCO_3^-]^\circ \cdot \frac{P_2S[P_1 + P_1P_2(S + 1)] + P_1P_2}{(1 + P_2S)[1 + P_1 + P_1P_2(S + 1)]} \tag{A12}$$

$$y = \frac{[HCO_3^-]^\circ}{1 + P_1 + P_1P_2(1 + S)} \tag{A13}$$

$$z = \frac{[M]}{K_M} \cdot P_2[HCO_3^-]^\circ \cdot \frac{P_1 + 2P_2S + P_1P_2S}{(1 + P_2S)[1 + P_1 + P_1P_2(S + 1)]} \tag{A14}$$

$$v = \frac{[Na]}{K_{Na}} \cdot P_2[HCO_3^-]^\circ \cdot \frac{P_1 + 2P_2S + P_1P_2S}{(1 + P_2S)[1 + P_1 + P_1P_2(S + 1)]} \tag{A15}$$

These values for x, y, z, and v are inserted into Eqs. A1–A5 to obtain values for the concentrations of the solutes after equilibrium has been achieved after the initial addition of HCO_3^-: $[CO_2]'$, $[HCO_3^-]'$, $[CO_3^=]'$, $[MCO_3]'$, and $[NaCO_3^-]'$.

It is instructive to examine the predictions of these equations for the standard HCO_3^--containing seawater that we use in our experiments. This solution normally contains 425 mM Na^+, 57 mM Mg^{++} and 3 mM Ca^{++}. We used the following parameter values:

$pK_1 = 6.1$	$K_M = 25$	$pH^\circ = 8.00$	[M] = 60 mM
$pK_2 = 10.0$	$K_{Na} = 170$	$[HCO_3^-]^\circ = 12$ mM	[Na] = 425 mM.

The value for pK_2 was chosen because, when used in the calculations for a solution lacking

Na^+, Ca^{++}, and Mg^{++} it led to a predicted pH change (i.e., $\sim+0.003$) that was very close to that observed when 12 mM HCO_3^- was added to a solution containing 425 mM *N*-methyl-D-glucammonium·Cl and 30 mM EPPS. Note that [M] = $[Mg^{++}]$ + $[Ca^{++}]$. The value chosen for K_M was selected because, when used in the calculations for a solution lacking Na^+ but containing 57 mM Mg^{++} and 3 mM Ca^{++}, it predicted a HCO_3^--induced pH change very close to that observed (i.e., -0.014). Finally, the value chosen for K_{Na} was selected because, when used in the calculations for a solution containing 425 mM Na^+, 57 mM Mg^{++} and 3 mM Ca^{++} it predicted a HCO_3^--induced pH change that was very close to that observed (i.e., ~-0.03) for our standard 12 mM HCO_3^- seawater.

To further test whether our estimates of pK_2, K_M, and K_{Na} were reasonable, we also computed the predicted pH changes for the addition of a wide range of amounts of HCO_3^- to seawaters initially at pH values ranging from 7.4 to 8.6. The observed values were always very close to those predicted by the model. For example, for pH 7.4, the model predicts that adding 12 mM HCO_3^- should cause pH to increase by 0.032, which is very close to the observed value. For a starting pH of 7.7, the model predicts that adding any amount of HCO_3^- will cause no pH change, which is our observation. At the other pH extreme, for an initial pH of 8.6, the model predicts that the addition of 12 mM HCO_3^- should cause pH to fall by 0.15, which is very similar to the observed value. Thus, on the basis of observed changes in pH caused by the addition of known amounts of HCO_3^- to defined solutions, the model appears consistent.

The aforementioned calculations only pertain to the first step of our solution-making process, in which the HCO_3^- is added to the ASW. If the initial pH exceeds 7.7, this addition of HCO_3^- causes a dose-dependent acidification. Coincidentally, $[CO_2]'$ is higher than the value that would obtain if the addition of HCO_3^- had not caused any pH change. The pH can be returned to its initial value by lowering $[CO_2]$. This can be achieved by gassing for an indefinitely long period with a gas mixture of the proper CO_2 content, or by briefly gassing with a CO_2-free solution until pH has been raised from pH′ to the initial value. In either case, CO_2 is lost to the gas phase, causing the equilibria to be shifted as follows:

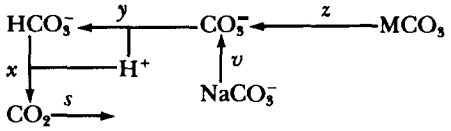

Scheme A2

where x, y, z, v, and s are fluxes through the indicated reactions. For initial pH values below 7.7, adding HCO_3^- causes an alkalinization, and $[CO_2]'$ is lower than if pH had not risen. pH can be returned from pH′ to pH° by gassing with a mixture having a CO_2 content greater than the ideal. The following derivation is independent of starting pH. At the final equilibrium,

$$[HCO_3^-]'' = [HCO_3^-]' + y - x \tag{A16}$$

$$[CO_3^=]'' = [CO_3^=]' + v + z - y \tag{A17}$$

$$[MCO_3]'' = [MCO_3]' - z \tag{A18}$$

$$[NaCO_3^-]'' = [NaCO_3^-]' - v \tag{A19}$$

$$[CO_2]'' = [CO_2]' + x - s \tag{A20}$$

$$pH'' = pH' + (x - y)/\beta \tag{A21}$$

where the double primes indicate the values prevailing after this second and final equilibrium is established. The following equations describe the four equilibria that are simultaneously established:

$$10^{(pH''-pK_1)} = \frac{[HCO_3^-]' + y - x}{[CO_2]' + x - s} \tag{A22}$$

$$10^{(pH''-pK_2)} = \frac{[CO_3^=]' + v + z - y}{[HCO_3^-]' + y - x} \tag{A23}$$

$$K_M = \frac{([CO_3^=]' + v + z - y)[M]}{[MCO_3]' - z} \tag{A24}$$

$$K_{Na} = \frac{([CO_3^=]' + v + z - y)[Na]}{[NaCO_3^-]' - v} \tag{A25}$$

By definition, the pH of the solution will be titrated back to pH°, so that pH″ = pH°. Manipulation of Eqs. A22–A25 leads to the following expressions for y, x, z, v, and s:

$$x = \frac{(P_1P_2 + 1)([CO_3^=]' + [NaCO_3^-]' + [MCO_3]') - P_2[HCO_3^-]'[1 - S + P_1P_2(S + 1)] - \beta(pH' - pH^\circ)[P_2(1 - S) + P_1P_2P_2(1 + S)]}{1 + P_1P_2} \tag{A26}$$

$$y = \frac{(P_1P_2 + 1)([CO_3^=]' + [NaCO_3^-]' + [MCO_3]') - P_2[HCO_3^-]'[1 - S + P_1P_2(S + 1)] - \beta(pH' - pH^\circ)[1 + P_2(1 - S) + P_1P_2 + P_1P_2P_2(1 + S)]}{1 + P_1P_2} \tag{A27}$$

$$z = [MCO_3]' - \frac{[M]}{K_M} \cdot [[HCO_3^-]' + \beta(pH' - pH^\circ)] \tag{A28}$$

$$v = [NaCO_3]' - \frac{[Na]}{K_{Na}} \cdot [[HCO_3^-]' + \beta(pH' - pH^\circ)] \tag{A29}$$

$$s = [CO_3^=]' - [[CO_2]' + [NaCO_3^-]' + [MCO_3]' - \frac{[HCO_3^-]'(1 + P_1P_2 + P_1P_2S) + \beta(pH' - pH^\circ)[1 + P_1P_2 + P_1(1 + SP_2)]}{P_1} \tag{A30}$$

These values for x, y, z, v, and s are inserted into Eqs. A16–A21 to obtain the solute concentrations obtaining after the final equilibrium has been achieved at the desired pH: $[CO_2]''$, $[HCO_3^-]''$, $[CO_3^=]''$, $[MCO_3]''$, and $[NaCO_3^-]''$.

It is instructive to examine the predictions of these equations for the case of our standard HCO_3^- ASW. As noted above, Eq. A11 correctly predicts that pH falls from 8.00 to 7.97 upon the addition of 12 mM HCO_3^-. Eqs. A26–A30 predict that as pH is returned to 8.00, 0.47 mM total CO_2 is lost to the atmosphere as CO_2. Furthermore, the final $[HCO_3^-]$ is 10.8 mM, and the final $[NaCO_3^-]$ is 269 μM. Thus, the actual $[HCO_3^-]$ is about 90% as large as the nominal $[HCO_3^-]$. The predicted error is increased slightly at lower amounts of added HCO_3^- (e.g., 88.7% of nominal for 0.75 mM added HCO_3^-), and decreased slightly at higher amounts of added HCO_3^- (e.g., 90.8% of nominal for 48 mM added HCO_3^-). The discrepancy between

actual and nominal [HCO_3^-] decreases as pH is decreased. This is expected, due to the decrease in ion-pair formation. For example, the addition of 12 mM HCO_3^- at pH 7.4 causes the predicted [HCO_3^-] to be 97.1% as large as the nominal [HCO_3^-], whereas the addition of a similar amount of HCO_3^- at pH 8.6 results in a predicted [HCO_3^-] that is only 71.6% of the nominal value.

APPENDIX 2

Analysis of Kinetic Models

Ion-pair model. Consider the following reaction sequence, in which DNDS and the $NaCO_3^-$ ion pair compete for binding to the carrier X:

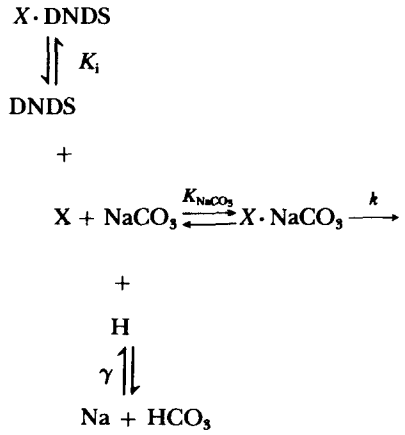

Scheme B1

where K_i, K_{NaCO_3}, and γ are equilibrium constants, and k is a rate constant describing the transport of $NaCO_3^-$ across the cell membrane. γ is defined as $[Na^+][HCO_3^-]/[NaCO_3^-][H^+]$), and has the value 1.7×10^6 M. Rapid equilibrium kinetics predicts the following:

$$J = \frac{[Na][HCO_3]J_{max}}{\gamma[H]K_{NaCO_3}(1 + [DNDS]/K_i) + [Na][HCO_3]}, \quad \text{(B1)}$$

which can in turn be rearranged to provide expressions for the experimentally determined parameters:

$$K_m(HCO_3^-) = K_{NaCO_3}\left(1 + \frac{[DNDS]}{K_i}\right)\frac{\gamma[H]}{[Na]} \qquad J_{max}(HCO_3^-) = J_{max} \quad \text{(B2, a and b)}$$

$$K_m(Na^+) = K_{NaCO_3}\left(1 + \frac{[DNDS]}{K_i}\right)\frac{\gamma[H]}{[HCO_3]} \qquad J_{max}(Na^+) = J_{max} \quad \text{(B2, c and d)}$$

We used a nonlinear least-squares method to fit the data of series 1–8 and A–D to Eq. B1, and obtained the best-fit values summarized in Table VI, line 1.

Random binding of Na^+ and HCO_3^-. Consider the reaction sequence in which DNDS,

HCO_3^-, and Na^+ all compete for binding to the carrier:

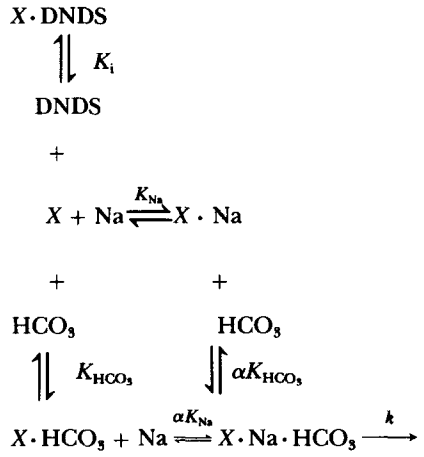

Scheme B2

where α describes how the binding of one substrate affects the affinity of the carrier for the other. Rapid-equilibrium kinetics predicts that:

$$J = \frac{[Na][HCO_3]J_{max}}{\alpha K_{Na}K_{HCO_3}(1 + DNDS]/K_i) + \alpha K_{HCO_3}[Na] + \alpha K_{Na}[HCO_3] + [Na][HCO_3]}, \quad \text{(B3)}$$

and the following expressions for the experimentally determined parameters:

$$K_m(HCO_3^-) = K_{HCO_3}\frac{\alpha K_{Na}\left(1 + \frac{[DNDS]}{K_i}\right) + \alpha[Na]}{\alpha K_{Na} + [Na]} \quad \text{(B4,a)}$$

$$J_{max}(HCO_3^-) = \frac{J_{max}[Na]}{\alpha K_{Na} + [Na]} \quad \text{(B4,b)}$$

$$K_m(Na^+) = K_{Na}\frac{\alpha K_{HCO_3}\left(1 + \frac{[DNDS]}{K_i}\right) + \alpha[HCO_3]}{\alpha K_{HCO_3} + [HCO_3]} \quad \text{(B4,c)}$$

$$J_{max}(Na^+) = \frac{J_{max}[HCO_3]}{\alpha K_{HCO_3} + [HCO_3]} \quad \text{(B4,d)}$$

We fitted the data of series 1–8 and series A–D to Eq. B3, and obtained the best-fit values summarized in Table VI, line 2. Given the result of the previous section, in which we showed that the data were fitted well by the ion-pair model, it is not surprising that the data are also fitted by the random-binding model. It is easily shown that the expressions for $K_m(HCO_3^-)$, $J_{max}(HCO_3^-)$, $K_m(Na^+)$ and $J_{max}(Na^+)$ of Eqs. B4, a–d (i.e., the random-binding model) reduce to the form of Eqs. B2, a–d (i.e., the ion-pair model) as α approaches zero under the restricted conditions in which: (*a*) the product $(\alpha K_{HCO_3}K_{Na})$ is fixed and (*b*) the quotient K_{Na}/K_{HCO_3} also is fixed. Thus, we might expect the best fit for the random-binding model to be achieved with a very small α and corresponding large values for K_{HCO_3} and K_{Na} expectations borne out by the fitting procedure.

The best-fit values for α, $K_{HCO_3^-}$ and K_{Na} predict apparent K_m and J_{max} values (Table IV, line 3) that are similar, but not identical, to those of the ion-pair model (Table IV, line 2). However, the predictions of the random-binding model should approach those of the ion-pair model more closely if α is decreased and K_{HCO_3} and K_{Na} compensatorily increased. For example, if (*a*) α is reduced by four orders of magnitude, (*b*) $K_{HCO_3^-}$ and K_{Na} are each raised by about two orders of magnitude, and (*c*) K_i is raised by ~55%, the predictions of the random-binding model are within 1% of those of the ion-pair model for our data.[2] Even if one considers Na^+ activation curves studied at $[HCO_3^-]_o$ values as high as 384 mM (eightfold higher than we used) with as much as 5 mM DNDS (20-fold higher), or HCO_3^- activation curves studied at $[Na^+]_o$ values as low as 13.25 mM (eightfold lower) with as much as 5 mM DNDS, the predictions of the random-binding model are within 2% of those of the ion-pair model. Thus, even if data obtained over a wide range of concentrations were to fit the ion-pair model perfectly, it would still be possible to fit the data nearly as well with a random-binding model.

Ordered binding of Na^+ then HCO_3^-. Consider the ordered reaction sequence in which DNDS competes with Na^+ for binding to the carrier:

$$\begin{array}{l} X\cdot\mathrm{DNDS} \\ \quad \Updownarrow K_i \\ \mathrm{DNDS} \\ + \\ X + \mathrm{Na} \overset{K_{Na}}{\rightleftharpoons} X\cdot\mathrm{Na} \\ \quad + \\ \quad \mathrm{HCO_3} \\ \quad \Updownarrow K_{HCO_3} \\ X\cdot\mathrm{Na}\cdot\mathrm{HCO_3} \xrightarrow{k} \end{array}$$

Scheme B3

Rapid-equilibrium kinetics predicts that:

$$J = \frac{[\mathrm{Na}][\mathrm{HCO_3}]J_{max}}{K_{Na}K_{HCO_3}(1 + [\mathrm{DNDS}]/K_i) + K_{HCO_3}[\mathrm{Na}] + [\mathrm{Na}][\mathrm{HCO_3}]}, \tag{B5}$$

and:

$$K_m(HCO_3^-) = K_{HCO_3}\frac{K_{Na}(1 + [\mathrm{DNDS}]/K_i) + [\mathrm{Na}]}{[\mathrm{Na}]} \qquad J_{max}(HCO_3^-) = J_{max} \quad \text{(B6, a and b)}$$

$$K_m(Na^+) = K_{Na}\frac{K_{HCO_3}(1 + [\mathrm{DNDS}]/K_i)}{K_{HCO_3} + [\mathrm{HCO_3}]} \qquad J_{max}(Na^+) = J_{max}\frac{[\mathrm{HCO_3}]}{K_{HCO_3} + [\mathrm{HCO_3}]} \quad \text{(B6, c and d)}$$

[2] For example, if $\alpha = 3 \times 10^{-6}$, $K_{HCO_3} = 6{,}920$, $K_{Na} = 43{,}350$, $K_i = 0.058$, and $J_{max} = 19.8$ pmol cm^{-2} s^{-1}, the predicted $K_m(HCO_3^-)$ values are 2.2 mM for series 1, 8.9 mM for series B, and 11.8 mM for series 3. Similarly, the predicted $K_m(Na^+)$ values are 78.5, 312, and 104 mM, respectively. The apparent J_{max} values range between 19.7 and 19.8 pmol cm^{-2} s^{-1}. Thus, all predictions are within 1% of those of the ion-pair model.

When we fitted the data of series 1–8 and series A–D to Eq. B5, we obtained the best-fit values summarized in Table VI, line 3. The fit provided by the Na^+-then-HCO_3^- ordered-binding model is to be expected, given the excellent fit of the ion-pair model, because it is easily shown that the predictions of this ordered-binding model (Eqs. B6, a–d) reduce to those of the ion pair model (Eqs. B2, a–d) as K_{HCO_3} approaches zero at a constant ($K_{HCO_3}K_{Na}$) product. Thus, we would expect the best fit of the Na^+-then-HCO_3^- ordered-binding model to be achieved with a very low K_{HCO_3} and a correspondingly high K_{Na}, as was indeed the case. The best-fit values for K_{HCO_3} and K_{Na} lead to predictions for the apparent K_m and J_{max} values (Table IV, line 4) that are similar, though not identical, to those of the ion-pair model (Table IV, line 2). However, if (*a*) $K_{HCO_3^-}$ is lowered by about two orders of magnitude, (*b*) K_{Na} is similarly raised, and (*c*) K_i is raised by ~25%, the predictions of the random-binding model are within 1% of those of the ion-pair model for our data.[3]

Ordered binding of HCO_3^- then Na^+. Consider the reaction sequence in which DNDS, HCO_3^-, and Na^+ all compete for binding to the carrier:

$$\begin{array}{ccc} X \cdot \text{DNDS} & & \\ \Updownarrow K_i & & \\ \text{DNDS} & & \\ + & & \\ X + HCO_3 & \overset{K_{HCO_3}}{\rightleftharpoons} & X \cdot HCO_3 \\ & & + \\ & & \text{Na} \\ & & \Updownarrow K_{Na} \\ & & X \cdot \text{Na} \cdot HCO_3 \xrightarrow{k} \end{array}$$

Scheme B4

Rapid-equilibrium kinetics predicts that:

$$J = \frac{[\text{Na}][HCO_3]J_{max}}{K_{Na}K_{HCO_3}(1 + [\text{DNDS}]/K_i) + K_{Na}[HCO_3] + [\text{Na}][HCO_3]}, \quad \text{(B7)}$$

and:

$$K_m(HCO_3^-) = K_{HCO_3}\frac{K_{Na}(1 + [\text{DNDS}]/K_i)}{K_{Na} + [\text{Na}]} \qquad J_{max}(HCO_3^-) = J_{max}\frac{[Na^+]}{K_{Na} + [Na^+]} \quad \text{(B8, a and b)}$$

$$K_m(Na^+) = K_{Na}\frac{K_{HCO_3}(1 + [\text{DNDS}]/K_i) + [HCO_3]}{[HCO_3]} \qquad J_{max}(HCO_3^-) = J_{max} \quad \text{(B8, c and d)}$$

[3] For example, if $K_{HCO_3} = 0.013$, $K_{Na} = 72{,}500$, $K_i = 0.058$, and $J_{max} = 19.8$ pmol cm^{-2} s^{-1}, the predicted $K_m(HCO_3^-)$ values are 2.2 mM for series 1, 8.9 mM for series B, and 11.8 mM for series 3. Similarly, the predicted $K_m(Na^+)$ values are 78.5, 312, and 104 mM, respectively. The apparent J_{max} values range between 19.7 and 19.8 pmol cm^{-2} s^{-1}. Thus, all predictions are within 1% of those of the ion-pair model.

We fitted the data of series 1–8 and series A–D to Eq. B7, obtaining the best-fit values reported in Table VI, line 4. As was the case for the random-binding model and the Na^+-then-HCO_3^- ordered-binding model, it is to be expected that the HCO_3^--then-Na^+ ordered-binding model would fit the data, given the excellent fit provided by the ion-pair model. It is easily demonstrated that the predictions of the HCO_3^--then-Na^+ ordered-binding model (Eqs. B8, a–d) reduce to those of the ion-pair model as K_{Na} approaches zero at a constant ($K_{HCO_3}K_{Na}$) product. As expected, the best fit of this model was achieved with a very low K_{Na} and a correspondingly high K_{HCO_3}. Although the best-fit values for K_{HCO_3} and K_{Na} predict apparent K_m and J_{max} values (Table IV, line 5) that are not identical to those of the ion-pair model (Table IV, line 2), the agreement is improved if K_{Na} is further reduced. For example, if (*a*) $K_{HCO_3^-}$ is increased by about two orders of magnitude, (*b*) K_{Na} is decreased by about two orders of magnitude, and (*c*) K_i is raised by ~20%, the predictions of the random-binding model are within 1% of those of the ion-pair model for our data.[4]

This work was supported by a grant from the National Institutes of Health, NH-18400. W. F. Boron was supported by a Research Career Development Award (DK-01022) and was a Searle Scholar during the time the research was carried out.

We thank Drs. John M. Russell and Gregory Boyarsky for helpful discussions, and Mrs. Eleanor Savage for her secretarial assistance.

Original version received 27 January 1988 and accepted version received 15 August 1988.

REFERENCES

Barzilay, M., and Z. I. Cabantchik. 1979. Anion transport in red blood cells. II. Kinetics of reversible inhibition by nitroaromatic sulfonic acids. *Membrane Biochemistry.* 2:255–281.

Boron, W. F. 1977. Intracellular pH transients in giant barnacle muscle fibers. *American Journal of Physiology.* 233:C61–C73.

Boron, W. F. 1985. Intracellular-pH-regulating mechanism of the squid axon: relation between the external Na^+ and HCO_3^- dependences. *Journal of General Physiology.* 85:325–345.

Boron, W. F., and R. C. Knakal. 1985. Intracellular-pH regulation by the squid axon: competition of DNDS, a reversible stilbene derivative, with external Na^+ and HCO_3^-. *Biophysical Journal.* 47:490*a*. (Abstr.)

Boron, W. F., W. C. McCormick, and A. Roos. 1981. pH regulation in barnacle muscle fibers: dependence on extracellular sodium and bicarbonate. *American Journal of Physiology.* 240:C80–C89.

Boron, W. F., and J. M. Russell. 1983. Stoichiometry and ion dependencies of the intracellular-pH-regulating mechanism in squid giant axons. *Journal of General Physiology.* 81:373–399.

Brinley, Jr., F. J., and L. J. Mullins. 1967. Sodium extrusion by internally dialyzed squid axons. *Journal of General Physiology.* 50:2303–2311.

Cabantchik, Z. I., P. A. Knauf, and A. Rothstein. 1978. The anion transport system of the red blood cell. The role of membrane protein evaluated by the use of 'probes'. *Biochimica Biophysica Acta.* 515:239–302.

[4] For example, if K_{HCO_3} = 6,600, K_{Na} = 0.143, K_i = 0.585, and J_{max} = 19.8 pmol cm^{-2} s^{-1}, the predicted $K_m(HCO_3^-)$ values are 2.2 mM for series 1, 8.9 mM for series B, and 11.7 mM for series 3. Similarly, the predicted $K_m(Na^+)$ values are 78.8, 315, and 104 mM, respectively. All apparent J_{max} values are ~19.8 pmol cm^{-2} s^{-1}. Thus, all predictions are within 1% of those of the ion-pair model.

Cabantchick, Z. I., and A. Rothstein. 1972. The nature of the membrane sites controlling anion permeability of human red blood cells as determined by studies with disulfonic stilbene derivatives. *Journal of Membrane Biology.* 10:311–328.

Fröhlich, O. 1982. The external anion binding site of the human ethythrocyte anion transporter: DNDS binding and competition with chloride. *Journal of Membrane Biology.* 65:111–123.

Garrells, R. M., M. E. Thompson, and R. Siever. 1961. Control of carbonate solubility by carbonate complexes. *American Journal of Science.* 259:24–45.

Hinke, J. A. M. 1967. Cation-selective microelectrodes for intracellular use. *In* Glass Electrodes for Hydrogen and Other Cations. Principle and Practice. G. Eisenman, editor. Marcel-Dekker, Inc., New York. 464–477.

Roos A., and W. F. Boron. 1981. Intracellular pH. *Physiological Reviews.* 61:296–434.

Russell, J. M., and W. F. Boron. 1976. Role of chloride transport in regulation of intracellular pH. *Nature.* 264:73–74.

Scarborough, J. B. 1966. Numerical Mathematical Analysis. Johns Hopkins University Press, Baltimore, MD.

Segel, I. H., 1975. Enzyme Kinetics. John Wiley and Sons, New York.

Thomas, R. C. 1976. Ionic mechanism of the H^+ pump in a snail neuron. *Nature.* 262:54–55.

Thomas, R. C. 1977. The role of bicarbonate, chloride and sodium ions in the regulation of intracellular pH in snail neurones. *Journal of Physiology.* 273:317–338.

Thomas, R. C. 1984. Experimental displacement of intracellular pH and the mechanism of its subsequent recovery. *Journal of Physiology.* 354:3P–22P.